Soft Matter

PAPER



Cite this: *Soft Matter*, 2021, **17**, 8937

# pH-Dependent complexation and polyelectrolyte chain conformation of polyzwitterion–polycation coacervates in salted water†

Kehua Lin, Benxin Jing and Yingxi Zhu *

Received 13th June 2021,
Accepted 9th September 2021

DOI: 10.1039/d1sm00880c

rsc.li/soft-matter-journal

The phase behavior and chain conformational structure of biphasic polyzwitterion–polyelectrolyte coacervates in salted aqueous solution are investigated with a model weak cationic polyelectrolyte, poly(2-vinylpyridine) (P2VP), whose charge fraction can be effectively tuned by pH. It is observed that increasing the pH leads to the increase of the yielding volume fraction and the water content of dense coacervates formed between net neutral polybetaine and cationic P2VP in contrast to the decrease of critical salt concentration for the onset of coacervation, where the P2VP charge fraction is reduced correspondingly. Surprisingly, a single-molecule fluorescence spectroscopic study suggests that P2VP chains upon coacervation seem to adopt a swollen or an even more expanded conformational structure at higher pH. As the hydrophobicity of P2VP chains is accompanied by a reduced charge fraction by increasing the pH, a strong pH-dependent phase and conformational behaviors suggest the shift of entropic and enthalpic contribution to the underlying thermodynamic energy landscape and chain structural dynamics of polyelectrolyte coacervation involving weak polyelectrolytes in aqueous solution.

## Introduction

Polyelectrolyte complex coacervates are liquid–liquid separated complex materials that are often formed between biological and/or synthetic polyelectrolytes bearing opposite charges in salt-added aqueous media. Polyelectrolyte complex coacervates and their underlying process of polyion association are ubiquitous in nature as being present in mussels, sandcastle worms, and other marine organisms.[1,2] Protein–polyelectrolyte coacervates have received much attention over the past decades as the coacervation between proteins and synthetic polyelectrolytes can be employed for effective protein separation and fractionation.[3,4] Since then, synthetic polyelectrolyte coacervates have been investigated not only for the fundamental understanding of the coacervation mechanism, but also for wide applications ranging from drug and gene delivery,[5–7] underwater adhesives,[8–10] to stimuli-responsive advanced functional nanomaterials.[2,7,11–14]

Despite widespread research on polyelectrolyte coacervates, the underlying thermodynamics of polyelectrolyte coacervation remains actively debated to date. Entropy driven ion-pairing accompanied by the release of counterions near polyelectrolytes to the bulk solution has been mostly accounted for polyelectrolyte coacervation.[2,12,15–21] Yet in some particular situations, such as high dielectric media or macroions bearing well-spaced charges, enthalpy contribution could be dominant as the driving force for polyelectrolyte coacervation.[18,22–24] Entropy-driven coacervate formation has been strongly regarded for coacervation between highly charged strong polyelectrolytes.[2,15,16,22] However, the mechanism becomes less clear and understood for the coacervation involving weak polyelectrolytes whose charge density is highly tunable by local ionic and pH environments and could even acquire charges from the solution, instead of counterion release.[18,22–24] Charge regulation and over-compensation on weak polyelectrolytes in aqueous solution of varied ionic and pH conditions[24–26] could significantly modify polyelectrolyte associative interactions and thereby the coacervate structure, leading to its strong pH- and ion-dependent phase behavior.[18,24] Additionally, hydrophobic interactions could also contribute considerably to charge association with weak polyelectrolytes of varied charge density, which could ultimately offset the entropy–enthalpy energy balance upon coacervation.[22,23,27,28] Yet with the nature of polymer chains, it is difficult to completely exclude the enthalpic contribution resulting from hydrophobic interactions between polyelectrolytes, except choosing multivalent ions[29] or inorganic macroions[30,31] as one building constitute component. However, the choice of hydrophilic polyions to form complex coacervates remains limited. Instead, chemical

*Department of Chemical Engineering and Materials Science, Wayne State University, Detroit, MI 48202, USA. E-mail: yzhu3@wayne.edu*

† Electronic supplementary information (ESI) available: Additional experimental results and data analysis (PDF). See DOI: 10.1039/d1sm00880c

approaches to further understand the thermodynamic landscape, in terms of relative entropic and enthalpic contributions, and to control the phase behavior of polyelectrolyte coacervate formation mostly rely on modifying the chemistry of polyelectrolyte monomers by different lengths of alkyl chains[32] or change density[27] or polarity,[28] *etc.* In this work, we instead take a simple and physical approach with a weak polyelectrolyte whose relative hydrophobicity can be varied by solution pH.

Furthermore, weak polyelectrolytes have grown as promising constituting material candidates to control the material properties of polyelectrolyte coacervates for broad applications thanks to their tunable charges and pH- and salt-responsive characteristics. Thus it is critical to understand the phase behavior and chain conformational structure of weak polyelectrolyte coacervates. Recent research has demonstrated that the material properties of polyelectrolyte complexes are intimately related to their microscopic structure including dynamic chain conformations.[2,15,28,33–39] The microstructures of dense polyelectrolyte coacervates have been characterized by different experimental techniques, such as small-angle scattering (including light scattering (SALS), X-ray scattering (SAXS), and neutron scattering (SANS)),[3,34,36–41] cryo-TEM and liquid TEM,[8,42–45] and fluorescence techniques.[4,12,46,47] The results obtained by dynamic light scattering, fluorescence recovery after photobleaching (FRAP), and TEM indicate a bifluidic sponge-like nanostructured network in polyelectrolyte dense coacervates, where structural heterogeneity is observed with domains of varied polymer density.[4] Conversely, recent results obtained by small-angle scattering experiments suggest that dense coacervates exhibit the behaviors of semi-dilute polymer solutions[46] or an interpenetrated overlapping gel-like network structure.[12,36,37,45] Nevertheless, most prior work has focused on the microstructure of polyelectrolyte coacervates formed with polyelectrolytes of fixed charge, yet the cases of polyelectrolyte coacervates with weak polyelectrolytes and the single-chain conformation of weak polyelectrolytes in the coacervates remain much less studied. Thus it remains an open question on how the dynamic conformational structure of weak polyelectrolytes is adopted upon coacervation in comparison to the original one before mixing. Limited results obtained *via* rheology and small-angle scattering indicate that the long polyelectrolyte chain dictates the overall microstructure of the dense coacervates.[41,48] However, the conformational structure of constitute polyelectrolytes strongly depends on their respective concentration ratios and solution ionic conditions and could remain nearly unchanged, or further unfolded or shrunk in comparison to that before coacervation. For example, recent studies indicate that some strong polyelectrolytes exhibit an ideal Gaussian chain conformation and the radius of gyration of these polyelectrolytes in dense coacervates is slightly larger than that in dilute solution.[41] Conversely, the conformation of polypeptides in coacervates could vary with the concentrations of both salt and the other oppositely charged constitute polyelectrolyte.[36] It is also expected that the conformational structure of polyelectrolytes, particularly weak polyelectrolytes, in coacervates could exhibit strong dependence on hydrophobic interactions or ''sticky'' contact in their chain chemistry and structure. Recent computer simulation work has predicted a distinct conformation change of a weak polyelectrolyte upon coacervation from that in solution.[18,23] Clearly, the conformational structure of polyelectrolytes upon coacervation remains debated and varies case by case with different polyelectrolytes and ionic environments of added polyions and salts. Yet, experimental investigation of the chain conformation of weak polyelectrolytes in their coacervates remains sparse. In this work, we focus on one model weak polyelectrolyte, whose chain conformation can be gradually modified by solution pH, in coacervation with a net neutral polyzwitterion that has little effect on the charge density of the weak polyelectrolyte.

In this work, we herein examine the coacervation and conformational structure of a weak polycation, poly(2-vinylpyridine) (P2VP) with a net neutral polyzwitterion, poly(dimethyl methacryloyloxyethyl ammonium propane sulfonate) (PDMAPS), in KCl-added aqueous solution of varied pH. Compared to other zwitterionic polymers, such as proteins and polyampholytes,[49] the net charge of selected PDMAPS is maintained to be absolutely zero without any excess charges from the polymer itself over the range of pH and salt concentration varied in this work,[50] thereby minimizing the charge regulation of P2VP by the other constitute polyelectrolyte in aqueous media. Thus it allows us to focus on the conformational change of P2VP upon its coacervation with PDMAPS in salted aqueous solution of varied pH. The pH- and salt-dependent conformational structures of P2VP chains in dilute aqueous solution have been well studied in the past[26,51,52] and can be used as reliable comparative references. Briefly, P2VP as a weak polybase becomes highly protonated at low pH and adopts a swollen coil structure in aqueous solution due to strong electrostatic repulsion between charged monomers. As its protonation degree decreases with increasing pH, the P2VP chain collapses at pH above a critical transition pH, $pH_{cr}$, and when weakened electrostatic repulsion becomes insufficient to overcome intra-chain hydrophobic attraction, the P2VP chain collapses sharply in dilute aqueous solution. Also adding salt to the P2VP aqueous solution could lead to a shift of its $pH_{cr}$ to a higher pH range than that in salt-free solution due to increased charge density. Yet it is challenging to characterize the chain conformation of weak polyelectrolytes in crowding complex environments, including the complex coacervate in this work, where ensemble-averaged experimental techniques, such as light or X-ray scattering, could become inapplicable due to the inhomogeneity of associative aggregations.[4,53] Therefore, we employ fluorescence correlation spectroscopy (FCS) to examine the conformational dynamics of fluorescence-labeled P2VP mixed in plain PDMAPS–P2VP complexes under varied solution conditions at the single-molecule level.[26,51,52] Hence, we first examine the phase behavior of PDMAPS–P2VP coacervates in KCl-salted aqueous solution with varied concentrations of PDMAPS, P2VP, and KCl and pH by fluorescence microscopy as well as titration for composition analysis. We then examine the conformational structure of a molecular fluorophore probe and fluorophore-labeled P2VP in the dense PDMAPS–P2VP

 

coacervates after removal of the supernatant. By using FCS, we determine the pH-dependent hydrodynamic size of P2VP chains upon PDMAPS–P2VP coacervation in comparison to that of P2VP in dilute aqueous solution. The understanding of the coacervation between the polyzwitterion and weak polyelectrolyte as well as the chain conformation in coacervates can be employed to control and develop ''smart'' novel materials for efficient ion exchange/transport, ultrafiltration, drug delivery, *etc.*[2,5–10,13,14,54]

# Experimental

### Materials

[2-(Methacryloyloxy)ethyl]dimethyl-(3-sulfopropyl)ammonium hydroxide (DMAPS), 2,2′-azobis-(2-methylpropionamidine)dihydrochloride (AAPH), acetone, potassium chloride (KCl), potassium chromate ($K_2CrO_4$), silver nitrate ($AgNO_3$), sodium chloride (NaCl), and sodium nitrate ($NaNO_3$) were all purchased from Sigma-Aldrich and used directly. Fluorophore probes, Alexa Fluor 488 succinimidyl ester (c-Alexa488, $\lambda_{ex}$ = 488 nm, Invitrogen), non-reactive Alexa Fluor 488 without any conjugation (n-Alexa488, $\lambda_{ex}$ = 488 nm, Invitrogen), and rhodamine 110 chloride (R110, $\lambda_{ex}$ = 488 nm, Sigma-Aldrich), were used directly.

P2VP of molecular weight $M_w$ = 24 000 g mol$^{-1}$ (polydispersity of $M_w/M_n$, PDI = 1.4) was synthesized by free radical polymerization[55] and repeatedly dissolved in ethanol and precipitated in water to lower the PDI. Amino-terminated P2VP of $M_w$ = 19 000 g mol$^{-1}$ (PDI = 1.3) was synthesized by reversible addition–fragmentation chain transfer polymerization[56] and subsequently covalently labeled with c-Alexa488 by following a prior protocol.[57,58] c-Alexa488 labeled P2VP as a fluorescent polymer probe (f-P2VP) is purified *via* dialysis in 0.1 M HCl for two weeks and freeze-dried before adding f-P2VP to unlabeled P2VP solution at a nanomolar level for the FCS experiment. After dialysis, f-P2VP dilute aqueous solution was also characterized by FCS to ensure no detectable free *c*-Alexa488 in the solution as shown in Fig. S1 (ESI†).

P2VP aqueous solutions of varied concentration were prepared by dissolving plain P2VP in HCl solution of known concentration ($\sim$0.2 M), at which P2VP becomes positively charged and dissolves well in aqueous solution. The pH of each P2VP solution was subsequently adjusted and monitored using a pH meter (Oakton pH6) until it reached a desired value. As p$K_a$ for weak polyelectrolyte changes with its surrounding environment, including the presence of charged small ions or macroions, it is difficult to measure it accurately. More complicatedly, the p$K_a$ of weak polyelectrolytes in aqueous solution is not a fixed value but over a range, whose broadness could strongly depend on the polyelectrolyte molecular weight and concentration. Hence, we have decided not to report the p$K_a$ of P2VP or use it in comparison to solution pH to estimate the charge density in the coacervate system. In this work, the charge fraction of P2VP monomers was calculated based on the actually consumed HCl amount in comparison to the 2VP monomer concentration based on the following chemical equilibrium: 2VP + $H^+$ $\rightarrow$ 2VP$^+$ and [2VP$^+$] + [$H^+$] = [added HCl], where the bracket refers to the concentration of each species. As the added HCl amount ($\sim$0.2 M) far exceeded the resulting pH (= 2.05–4.37) of P2VP solution, we estimated the charge fraction, $\alpha \approx$ [added HCl]/[2VP].

The pH of PDMAPS aqueous solutions before mixing was also adjusted by varying the added amount of HCl stock solution of pH = 2.0 and measured using a pH meter. It should be noted that the control of solution pH by adjusting the concentration of strong acid, such as HCl, instead of using buffer solutions, has minimal effect on undesired electrostatic screening. The pH values reported in this work were all measured in polymer solutions before equal volumetric mixing for coacervation. Yet it should be pointed out that as P2VP is a weak polybase and actually works as a buffer agent in water, its solution pH changed very little upon dilution or mixing with PDMAPS. Hence, the final pH of the coacervates was approximate to the pH of P2VP and PDMAPS solutions before mixing.

The PDMAPS polymer was synthesized by solution polymerization by following a published procedure,[31,49] except that the monomer was different. To prepare a homogeneous PDMAPS aqueous solution at room temperature, KCl was added to significantly lower the upper critical solution temperature (UCST) of PDMAPS to be below 0 °C and eliminate the ''self-coacervate'' complexation of PDMAPS itself.[7,50,59,60] In this work, when the KCl concentration in the PDMAPS aqueous solution was greater than 50 mM, no phase separation due to UCST was observed at $T > 0$ °C, ensuring the initial homogeneous PDMAPS solution.

### Preparation and characterization of PDMAPS–P2VP coacervate complexes

To control the formation of complex coacervates, KCl was added to both P2VP and PDMAPS stock solutions at the same concentration before mixing. By varying the molar ratio of the total 2VP monomers to total DMAPS monomers in the aqueous mixture of PDMAPS/KCl and P2VP/KCl solutions, the formation of PDMAPS–P2VP biphasic complex coacervates was examined. The phase behavior and morphology of the PDMAPS–P2VP complex formed after mixing two polymer solutions were further examined using a confocal laser scanning microscope (CLSM, Carl Zeiss LSM 780) using a 63× objective lens (Plan-Apochromat, NA = 1.4, oil immersion) and an Airyscan detector (Carl Zeiss), for which n-Alexa488 was added to the P2VP/KCl solution at an n-Alexa488 : 2VP molar ratio of 1 : 1000 in aqueous solutions. All the characterization reported in this work was carried out at constant temperature, $T$ = 23 °C.

The yielding volume fraction of dense coacervates after thorough removal of supernatant solutions was determined using a procedure as follows. After the formation of biphasic coacervates, the mixture was left to rest overnight before separation. To thoroughly remove trace droplets of polymer-poor supernatant solution from the dense coacervate, the mixture was centrifuged at 10 000 g for 30 min at $T$ = 23 °C and left overnight before the top supernatant solution was removed. The extracted supernatant was weighed using a

balance with a measurement uncertainty of ±0.001 g. Considering that the supernatant appeared to be very dilute aqueous solution with polymers in low concentrations, we simply assumed its density in approximation to that ($\approx$1 g ml$^{-1}$) of water and calculated the volume of the supernatant phase accordingly, which appeared consistent with the roughly measured volume using a pipette upon extraction. It is noted that the weight measurement of extracted supernatant solution is more accurate than the volume measurement in this work, particularly when the volume of the supernatant solution is rather small. Accordingly, the yielding volume and volume fraction of the dense coacervate were obtained by subtracting the volume of the extracted supernatant solution from the total volume (= 800 μl) of the mixture, for which we observed no noticeable volume expansion or contraction upon mixing.

To determine the water content in the PDMAPS–P2VP dense coacervates, the wet dense coacervates after the removal of their corresponding supernatant solutions were weighed and then freeze-dried over 16 h. The weight fraction of water in the dense coacervate was determined by subtracting the mass of the dried dense coacervate from that of the initial wet coacervate of known mass at each solution condition.

The concentrations of KCl in the dense and supernatant phases were determined based on the titration of $Cl^-$ ions in the supernatant solution. The extracted supernatant after centrifugation from biphasic PDMAPS–P2VP coacervates was directly titrated by $AgNO_3$ solution using $K_2CrO_4$ as the indicator (aka, Mohr's method).[61,62] Mohr's method is an extremely sensitive and accurate method to determine chlorine concentration with a relative standard deviation $\leq$0.07%.[63] $AgNO_3$ solution was first titrated by a standard NaCl solution to calibrate its concentration. The titration measurement for each supernatant solution was repeated three times. With the known yielding volume of the dense coacervate and the total amount of $Cl^-$ ions, including both the added KCl salt and HCl for pH adjustment, the concentration of the $Cl^-$ ions in the dense coacervate was calculated. The concentrations of P2VP in the dense and supernatant phases were determined using a UV-vis spectrophotometer (V-630, JASCO). The control experiment showed that the intensity of the characteristic UV-vis absorbance peak of plain protonated P2VP at a wavelength of 260 nm[56] increases with P2VP concentration in aqueous solution, yielding a calibrated linear relationship of the P2VP concentration against UV-vis characteristic peak intensity (see Fig. S2, ESI†). The separated supernatant solution after centrifugation was diluted $\sim$1000 times to ensure that the concentration of the sample was in the range of the calibration curve. The concentration of P2VP in the supernatant solution was thereby obtained by comparing the measured absorbance intensity to that of the calibration one. Similarly, with the known yielding volume fraction of the dense coacervate and the total amount of P2VP, the concentration of P2VP in the dense coacervate was calculated accordingly.

FCS was employed to determine the conformational structure of P2VP in dense PDMAPS–P2VP coacervates formed at varied pH. The diffusion coefficient, $D$, and thereby the hydrodynamic radius, $R_H$, of hydrophilic R110 and f-P2VP probes in the dense coacervates were obtained by FCS. The FCS setup was based on an inverted microscope (Zeiss Axio A1) equipped with an oil-immersion objective lens (Plan Apochromat 100×, NA = 1.4). Briefly, the tiny fluctuation, $I(t)$, in fluorescence intensity, due to the motion of fluorescent probes in and out of the laser excitation volume of a solid-state blue laser (Crystal Laser, $\lambda_{ex}$ = 488 nm), was measured by two single photon counting modules (Hamamatsu) independently in a confocal detection geometry at a sampling frequency of 100 kHz in this work. The autocorrelation function, $G(\tau)$, of measured $I(t)$ as[64,65]

$$G(\tau) = \langle \delta I(t) \times I(t+\tau) \rangle / \langle I(t) \rangle^2 \quad (1)$$

was thereby obtained by using a multichannel FCS data acquisition system (ISS) *via* cross-correlation analysis, which removed the artifacts from detectors. The dimension of the excitation confocal volume was calibrated as $\omega \approx 288$ nm in the lateral radius and $z \approx 5$ μm in the vertical half-height by n-Alexa488 of known $D$ (= 435 μm$^2$ s$^{-1}$) at a $10^{-9}$ M molar concentration in aqueous solution. The $D$ and concentration, [C], of the fluorescent probe can be obtained from the fitting of $G(\tau)$ based on a given equation as detailed in the section of Results and discussion below. The conformational structure, described by the hydrodynamic radius, $R_H$, of the f-P2VP chain in the PDMAPS–P2VP dense coacervates of varied polymers and salt concentrations and pH was obtained by naïvely employing the Stokes–Einstein equation to the measured diffusion coefficient as

$$R_H = \frac{k_B T}{6\pi\eta D}, \quad (2)$$

where $k_B$ is the Boltzmann constant and $\eta$ is the known viscosity of the medium. All the measurements reported in this work were repeated at least three times for each sample.

## Results and discussion

We start by investigating the pH-dependent coacervate formation between zwitterionic PDMAPS and cationic P2VP in KCl aqueous solution of fixed total DMAPS and 2VP monomer concentration, $c_T$ = 0.2 M. It is noted that both PDMAPS–KCl and P2VP–KCl aqueous solutions at pH = 2.05–4.37 are homogenous and transparent before mixing, while their mixtures exhibit distinct phase behaviors with dependence on the 2VP-to-total monomer molar ratio, $c_{2VP}/c_T$, KCl concentration, $c_{KCl}$, and pH. As shown in Fig. 1a, at $c_{KCl}$ = 0.1 M and pH = 2.05 at which P2VP is highly protonated in aqueous solution, the mixture spontaneously separates into two transparent liquid phases with one clear dilute supernatant upper phase and the other clear dense coacervate phase on the bottom of the glass vial when $c_{2VP}/c_T$ exceeds 5%. It is noted that despite easily observable liquid–liquid separation, all the dense coacervates formed at varied $c_{2VP}/c_T$, $c_{KCl}$, and pH in this work appear to be transparent without detectable cloudiness by the naked eye, suggesting low viscosity and high water content in the dense

 

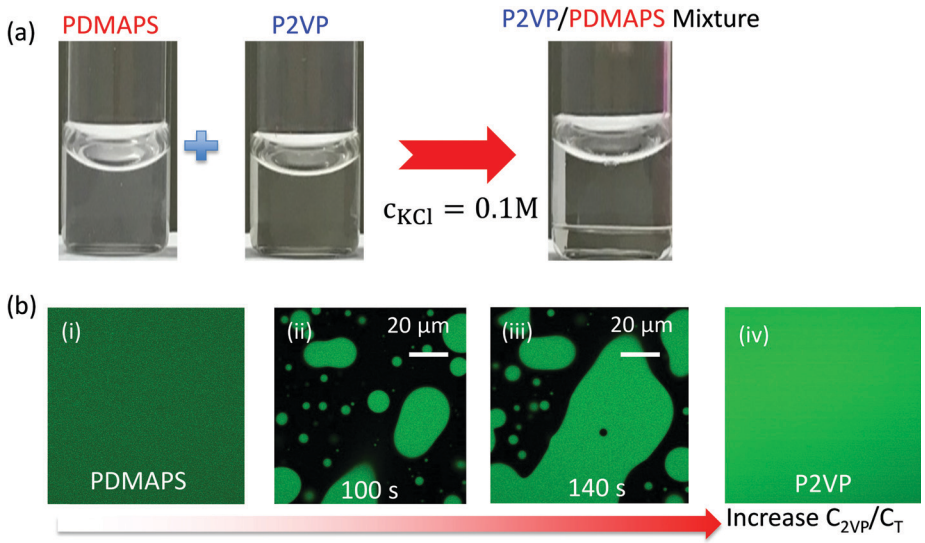


Fig. 1 (a) Representative optical photographs of PDMAPS and P2VP aqueous solutions, both added with. $c_{KCl}$ = 0.1 M, and liquid–liquid separated PDMAPS–P2VP coacervates formed at $c_{2VP}/c_T$ = 0.25 and pH = 3.04. (b) Fluorescence micrographs of (i) PDMAPS and (iv) P2VP solution and (ii) and (iii) PDMAPS–P2VP coacervate formed under the same conditions as shown in (a) acquired at elapsed times of (ii) 100 s and (iii) 140 s after mixing.

coacervates (see Fig. 3b) and weak association between PDMAPS and P2VP for coacervate formation as further discussed below.[12,22] We verify the biphasic PDMAPS–P2VP coacervate formation and determine its phase diagram by CLSM with n-Alexa488 added to the mixture. At $c_{2VP}/c_T \leq \sim 0.05$ and $\geq \sim 0.95$, the morphology of PDMAPS–P2VP mixtures appears to be homogeneous and featureless as shown in fluorescence micrographs in Fig. 1b(i) and (iv), respectively. As shown in Fig. 1b(ii) and (iii) for the complex formed at $c_{2VP}/c_T$ = 0.25 and added with n-Alexa488, we observe that the fluorescent droplets of the dense coacervate phase are dispersed in the non-fluorescent dilute supernatant solution, exhibiting the hallmark of the emulsion-like morphology of biphasic complex coacervates.[8,27,31,35,66] As n-Alexa488 is negatively charged and can strongly interact with cationic P2VP, it strongly suggests that the fluorescent dense phase is the polymer-rich phase while the non-fluorescent dilute supernatant is the polymer-poor phase. Over elapsed time, the fluorescence droplets could coalesce with each other and expand into a fractal and space-spanning morphology as shown in Fig. 1b(ii) and (iii), confirming the liquid-like nature of polyelectrolyte complex coacervates.

In this work we vary the pH of polymer solutions from pH = 2.05–4.37. A similar emulsion-like morphology is confirmed as shown in Fig. S3, ESI.† As both the P2VP monomer concentration ($\sim$0.01–0.19 M) and added HCl amount to adjust the final solution pH are higher than the final proton concentration in the solution, we can estimate the charge fraction, $\alpha$, of P2VP based on the ratio of consumed HCl to 2VP concentration. For instance, at $c_{2VP}/c_T = \sim 0.25$, $\alpha$ is estimated to change from 65% to 30% with increasing pH from 2.05 to 4.37, respectively (as also shown in Fig. 2b and 3b). Biphasic PDMAPS–P2VP coacervates can be formed over pH = 2.05–4.37. Yet the critical $c_{2VP}/c_T$ and $c_{KCl}$ for the coacervate formation

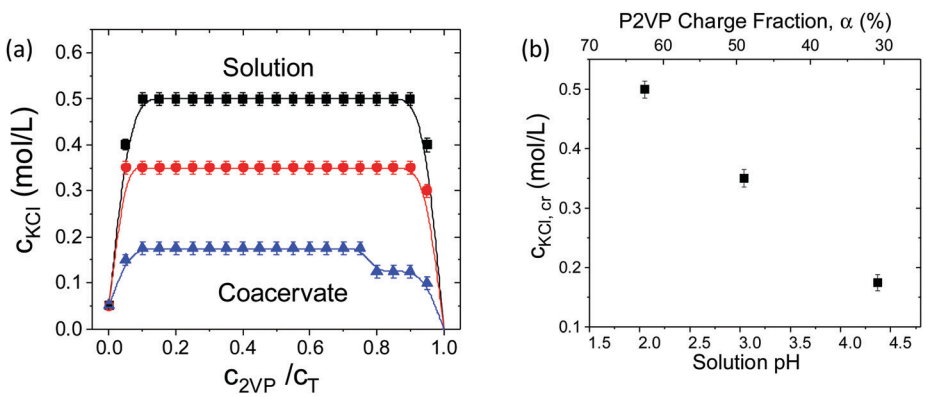


Fig. 2 (a) Effect of pH on the phase diagram of PDMAPS–P2VP coacervate formation at $c_{2VP}/c_T$ = 0.25, $c_T$ = 0.2 M, and $c_{KCl}$ = 0.1 M but varied pH = 2.05 (black squares), 3.04 (red circles), and 4.37 (blue triangles). (b) Upper critical salt concentration for PDMAPS–P2VP coacervate formation at $c_{2VP}/c_T$ = 0.25 and $c_T$ = 0.2 M against solution pH (bottom $x$-coordinate axis) and resulting charge fraction, $\alpha$ of P2VP (top $x$-coordinate axis).

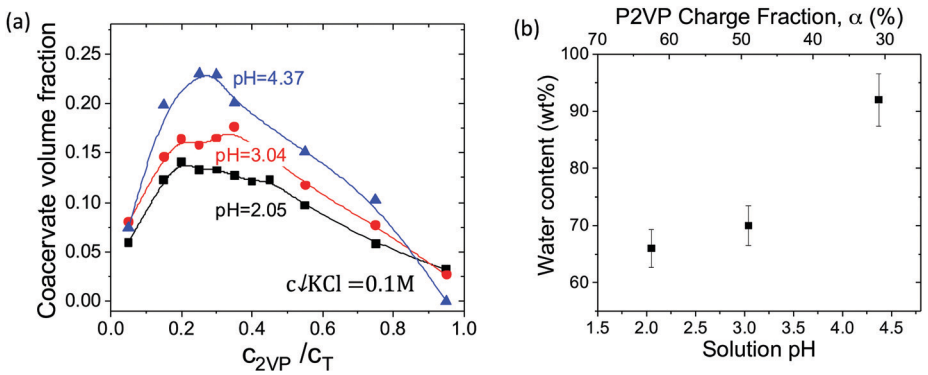


Fig. 3 (a) Yielding volume fraction of PDMAPS–P2VP dense coacervates against $c_{2VP}/c_T$ for coacervates formed at fixed $c_T$ = 0.2 M and $c_{KCl}$ = 0.1 M but varied pH = 2.05 (black squares), 3.04 (red circles), and 4.37 (blue triangles) after removal of the supernatant solution. (b) Weight fraction of water in the dense coacervates against solution pH (bottom *x*-coordinate axis) and resulting charge density of P2VP (top *x*-coordinate axis). Water content was measured after freezing–drying the separated wet dense coacervates from the supernatant. The coacervates were formed at $c_{2VP}/c_T$ = 0.25, $c_T$ = 0.2 M and $c_{KCl}$ = 0.1 M.

show strong dependence on pH. We determine the phase diagram of PDMAPS–P2VP complex formation in salted aqueous solution against $c_{2VP}/c_T$, $c_{KCl}$ and pH as summarized in Fig. 2a. In this work, at the lowest $c_{KCl}$ = 0.05 M that ensures to fully dissolve PDMAPS in aqueous solutions at room temperature, we observe that the PDMAPS–P2VP complex coacervates can be formed over a wide range of $c_{2VP}/c_T$ = ~0.05–~0.95 without any noticeable precipitation. The polymer concentration range for PDMAPS–P2VP coacervation appears to be much broader than that reported for conventional polyanion–polycation coacervates where one polymer component-to-total polymer ratio typically ranges from 20% to 80%.[22,67–70] Such a wide polyelectrolyte concentration range is similar to that of coacervates formed with zwitterionic polyelectrolytes.[30,31,71] We attribute the broad coacervate phase to the ionic effect on the charge density, despite being maintained net neutral, of PDMAPS, which increases with increasing simple ion or macroion concentration due to enhanced ion binding with dipolar DMAPS monomers.[60] In this work, we expect that such charge regulation of PDMAPS could also involve P2VP as a cationic macroion, which further complicates the case here considering its own weak polyelectrolyte nature as discussed below. The upper critical KCl salt concentration, $c_{KCl,cr}$, above which a transition from a biphasic coacervate to monophasic solution occurs, is determined by CLSM. It is clearly shown in Fig. 2b that increasing pH at a given $c_{2VP}/c_T$ leads to a considerable decrease of $c_{KCl,cr}$, indicating that the coacervate phase is narrowed. Such a trend is consistent with previous studies of pH-dependent polyelectrolyte coacervation with weak polyacids and/or weak polybases[22,68] due to pH-induced variance in the charge density of weak polyelectrolytes. The monotonic decrease of $c_{KCl,cr}$ with increasing pH from 2.05 to 4.37 (or correspondingly decreasing P2VP charge fraction) is consistent with the trend reported with the coacervates using weak polyelectrolytes of varied charge density, which is strongly correlated with entropic driving force, directly resulting from the number of released bound ions in close vicinity to polyelectrolytes upon their ion pairing.[22,68]

We also examine the yielding volume fraction of PDMAPS–P2VP dense coacervates against $c_{2VP}/c_T$ and pH at constant $c_{KCl}$ = 0.1 M as shown in Fig. 3a. It is interesting to observe that the yielding volume fraction of dense coacervates exhibits a non-monotonic change with increasing $c_{2VP}/c_T$ at all three varied pHs, where the total volume and total monomer concentration of two polymer solutions before mixing are kept constant. At low $c_{2VP}/c_T < 0.2$, the yielding volume fraction of the dense coacervate phase increases with increasing P2VP concentration. Upon further increasing the P2VP concentration, the yielding volume fraction of dense coacervates decreases considerably. The maximum yielding volume of the PDMAPS–P2VP dense coacervates is found at $c_{2VP}/c_T \sim 0.2$–0.3 for varied pH. The non-monotonic and asymmetric change of the yielding volume of dense coacervates with $c_{2VP}/c_T$ suggests that the interaction and structure of the PDMAPS–P2VP coacervates vary with P2VP and PDMAPS concentrations, possibly due to varied charge density and resulting conformational change of P2VP and PDMAPS upon association. As a result, an optimal $c_{2VP}/c_T$ at each given pH for maximizing PDMAPS–P2VP ion pairs is present. As the charge density and conformational structure of P2VP could be more strongly affected by pH and local ionic conditions than net-neutral zwitterionic PDMAPS, the asymmetric change with $c_{2VP}/c_T$ at constant $c_T$ could be expected. Furthermore, at all varied $c_{2VP}/c_T$, except the extremely low and high limits, the yielding volume fraction of the PDMAPS–P2VP dense coacervates increases by nearly 50% with increasing pH from 2.05 to 4.37. As the P2VP chain becomes less swollen with increasing pH[51,52] while the PDMAPS chain conformation changes negligibly at pH > 1,[60,70] we exclude the contribution of polymer chain swelling to the increased yielding volume of dense coacervates. Additionally, we determine that the water content in dense coacervates at constant $c_{2VP}/c_T$ = 0.25 and $c_{KCl}$ = 0.1 M, where the maximum yielding volume of dense coacervates is obtained, also increases with increasing pH as shown in Fig. 3b. Such a trend appears opposite to the reported increase of water content in polyelectrolyte coacervates with increased polyelectrolyte charge density due to enhanced

 

Table 1 List of charge fraction of P2VP, critical KCl concentration for the onset of coacervation, yielding volume fraction, and water content of dense coacervates at varied pH

| | Charge fraction, $\alpha$ of P2VP (%) | $C_{KCl,cr}$ (mol $L^{-1}$) | Yielding volume fraction of dense coacervate (%) | Water content of dense coacervates (%) |
|---|---|---|---|---|
| pH = 2.05 | 65 | 0.50 | 23.0 | 66 |
| pH = 3.04 | 50 | 0.35 | 15.8 | 70 |
| pH = 4.37 | 30 | 0.20 | 13.3 | 92 |

electrostatic association.[22] To further examine the pH-effect, we have also summarized the pH-dependent solution conditions of the PDMAPS–P2VP coacervates formed at constant $c_T$ = 0.2 M, $c_{2VP}/c_T$ = 0.25, and $c_{KCl}$ = 0.1 M in Table 1. The concomitant increase of yielding volume fraction and water content of the PDMAPS–P2VP dense coacervates suggests the strong effect of P2VP chain hydrophobicity on the thermodynamics and structure of PDMAPS–P2VP association upon coacervation. As suggested by theoretical predictions, the "sticky" hydrophobic interaction between PDMAPS and P2VP could offset the weakened entropic-driven ion-pairing between P2VP and PDMAPS to some degree. Enhanced hydrophobic interactions could also lead to the exclusion of more interfacial water in close vicinity to both polyelectrolytes upon their aggregation.[22,23,27,28,72,73] Alternatively, the increase of water content in the PDMAPS–P2VP dense coacervate at high pH could be attributed to a lower associative networking degree due to the reduced charge density of P2VP, which is analogous to increased water uptake by a reduced crosslinking degree of the hydrogel.[74] Nevertheless, we speculate that the enthalpic contribution to the thermodynamics underlying PDMAPS–P2VP coacervation could be increased with respect to reduced entropic contribution due to a lower charge density of P2VP at higher pH, despite the weakening of the total PDMAPS–P2VP associative interaction.[33,66,75]

The pH-induced shift of the thermodynamic energy landscape, in terms of relative entropic and enthalpic contribution, for PDMAPS–P2VP coacervate formation is supported by the measured compositions of P2VP and KCl in dense and supernatant phases as shown in Fig. 4. With the known respective yielding volumes of the supernatant and dense phases, the molar concentrations of P2VP and KCl in each phase are measured against pH in comparison to their initial concentrations of $c_{2VP}/c_T$ = 0.25 and $c_{KCl}$ = 0.1 M as shown in Fig. 4a and b, respectively. At low pH = 2.05 where P2VP is highly protonated, the measured $c_{2VP}$ in the dense coacervate phase is indeed higher than that in the supernatant phase, yet $c_{KCl}$ is lower, strongly supporting entropy-driven coacervate formation resulting from the release of interfacial bound ions near the polyelectrolytes upon PDMAPS–P2VP binding. However, upon increasing the pH, the P2VP concentration in the supernatant phase clearly exhibits a monotonic increase by more than one order of magnitude to approach its original concentration before mixing. In contrast, a moderate decrease of P2VP concentration in the dense phase is observed with increasing pH. Conversely, the KCl concentration in dense coacervates also exhibits a monotonic increase with increasing pH to approach its initial concentration in solution while its concentration in the supernatant phase exhibits nearly pH-independence and approximates to the initial concentration, $c_{KCl}$ = 0.1 M. Mostly intriguingly, at pH = 4.37, the P2VP concentrations in both phases appear to converge toward its initial concentration, indicating nearly equal partition of P2VP in both phases. Thus, considerable reduction of the concentration gap between the supernatant and dense coacervate phases with increasing pH strongly suggests much weakened entropic contribution to PDMAPS–P2VP coacervate formation. Importantly, this suggests that complex coacervation involving weak polyelectrolytes can be tuned by pH, leading to associative polyion binding of varied strength.[27,28,48,70,72]

Next, we investigate the pH effect on the dynamic conformational structure of the P2VP chain upon its coacervation with PDMAPS in KCl aqueous solutions. As the molecular weight of PDMAPS is much higher than that of P2VP, it is generally regarded that the overall structure of non-stoichiometric PDMAPS–P2VP dense coacervates is mainly governed by long PDMAPS chains.[41,47] In this work, we thereby focus on

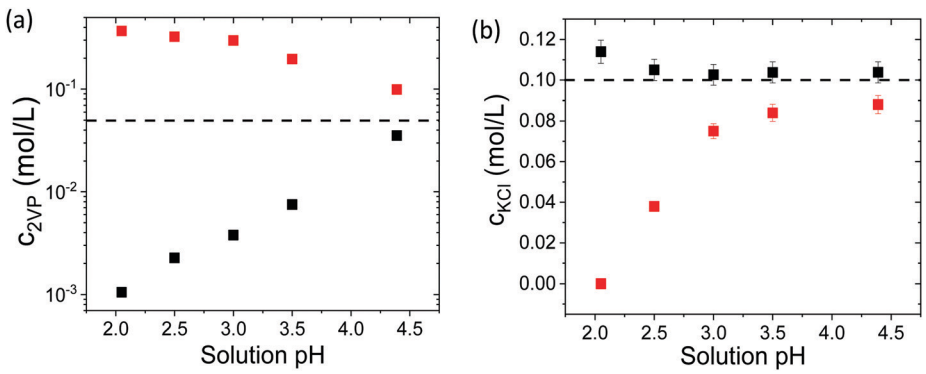


Fig. 4 Measured molar concentrations of (a) 2VP monomer and (b) KCl in the supernatant (black squares) and dense coacervate (red squares) against solution pH for PDMAPS–P2VP coacervates formed at $c_T$ = 0.2 M, $c_{2VP}/c_T$ =0.25, and $c_{KCl}$ = 0.1 M in comparison to their respective initial concentration before mixing (dashed line).

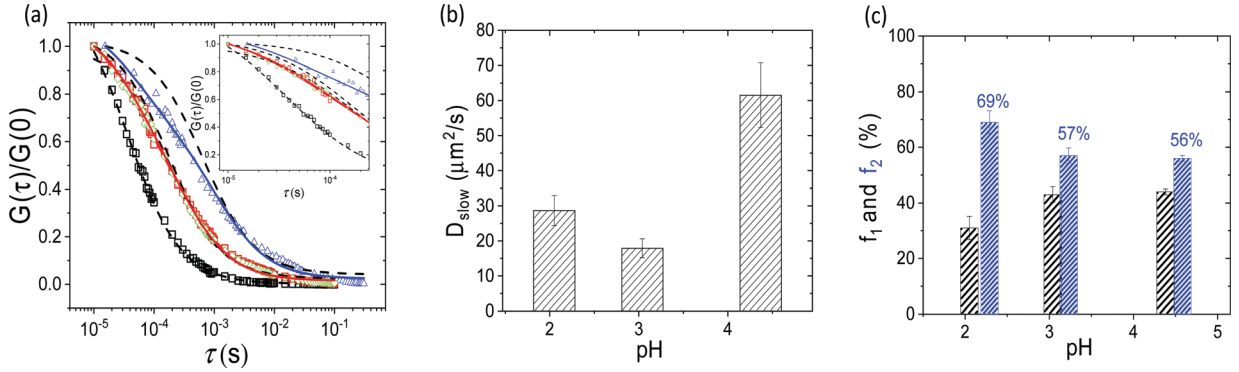


Fig. 5 (a) Normalized autocorrelation functions, $G(\tau)$ by $G(0)$ of R110 in PDMAPS–P2VP dense coacervates formed at pH = 2.05 (red circles), 3.04 (green triangles), and 4.37 (blue diamonds) in comparison to that in dilute aqueous solution of the same $c_{KCl}$ and pH (black squares). Black dashed line indicates the fitting with eqn (3) while solid line indicates the fitting with eqn (4). Inset: The blowout of $G(\tau)/G(0)$ at short $\tau$ to emphasize the deviation of the fitting using eqn (3). (b) Obtained $D_{slow}$ (red column) of R110 in PDMAPS–P2VP dense coacervates formed at different pHs. (c) Fitting parameter $f_1$ (black column) and $f_2$ (blue column) corresponding to $D_{fast}$ and $D_{slow}$, respectively.

the pH-dependent conformational structure of P2VP in the PDMAPS–P2VP dense coacervates at fixed $c_{2VP}/c_T$ = 25% and $c_{KCl}$ = 0.1 M by determining its diffusive dynamics using FCS at the single-molecule level. We carry out the control experiment of hydrophilic, positively charged R110 in the PDMAPS–P2VP dense coacervates to examine the diffusive dynamics of simple molecular probes in a complex coacervate environment.[57,76] As shown in Fig. 5a, the measured $G(\tau)$ of R110 in the dense coacervate apparently shifts to longer lag time in comparison to that in polymer-free dilute aqueous solution, indicating slower diffusive dynamics in the dense coacervate due to its higher viscosity than that in polymer-free water. For the control case of R110 in polymer-free dilute aqueous solution, the measured $G(\tau)$ normalized by $G(\tau = 0)$ measured can be perfectly fitted by the equation:

$$G(\tau) = \left([c]\pi^{1.5} z\omega^2\right)^{-1}\left(1+\frac{4D\tau}{\omega^2}\right)^{-1}\left(1+\frac{4D\tau}{z^2}\right)^{-0.5} \quad (3)$$

assuming simple three-dimensional Brownian motion,[51,52,65] yielding $D$ = 520 μm$^2$ s$^{-1}$ in good agreement with the known $D$ (= 470 μm$^2$ s$^{-1}$) for R110 in deionized water within FCS experimental uncertainty.[57,76] However, the fitting of measured $G(\tau)/G(0)$ for R110 in PDMAPS–P2VP dense coacervates by eqn (3) shows considerable deviation in a low $\tau$ range as the blown-out is shown in the inset of Fig. 5a. Such a fitting deviation is observed with R110 in the dense coacervates formed at varied pH, indicating that a simple Brownian dynamics of R110 with one single diffusion coefficient becomes inaccurate and inapplicable to describe the structural dynamics of the P2VP chain in the dense coacervates. The deviation from eqn (3) at short lag time often suggests the presence of a fast diffusive dynamics in the complex environment.[4,65,77] It is noted that the deviation from eqn (3) is distinct from recently reported sub-diffusive molecular transport in specific protein–DNA coacervates, which is observed by varying the optical observation size from ~50–224 nm and attributed to a specific charge–π interaction in the coacervate system.[78] Conversely, in our FCS setup, our observation spot size is fixed at $\omega$ = 288 nm. More importantly, we expect that merely electrostatic charge–charge and hydrophobic interactions are present in our PDMAPS–P2VP coacervates. Measured $G(\tau)$ results by our FCS show the Brownian diffusion of two distinct species in PDMAPS–P2VP dense coacervates, different from the Fickian diffusion dynamics reported elsewhere.[78] Accordingly, we have tentatively fitted the measured $G(\tau)$ with the model including two distinct dynamic species by using the following equation:

$$G(\tau) = \left([c]\pi^2 z^2\omega^2\right)^{-1}\left[f_1\left(1+\frac{4D_{fast}\tau}{\omega^2}\right)^{-1}\left(1+\frac{4D_{fast}\tau}{z^2}\right)^{-0.5} + f_2\left(1+\frac{4D_{slow}\tau}{\omega^2}\right)^{-1}\left(1+\frac{4D_{slow}\tau}{z^2}\right)^{-0.5}\right] \quad (4)$$

where $f_1$ and $f_2$ (= 1 − $f_1$) are the molar fractions corresponding to $D_{fast}$ and $D_{slow}$, respectively. According to the previously reported sponge-like microstructure of polyelectrolyte complex coacervates,[4,46,79] we expect that $D_{fast}$ corresponds to the diffusion of R110 in aqueous medium between PDMAPS–P2VP associated complex domains, essentially similar to that in dilute aqueous solution, and thereby set $D_{fast}$ = 520 μm$^2$ s$^{-1}$. It is noted that the variance of obtained $D_{slow}$ and $f_2$ by varying the value of $D_{fast}$ from 470–520 μm$^2$ s$^{-1}$ for the fitting with eqn (4) is smaller than 3%, which is far below the FCS experimental uncertainty, and thereby negligible. The extracted $D_{slow}$, which corresponds to the diffusion of R110 in the PDMAPS–P2VP associative network, and its corresponding $f_2$ are summarized in Fig. 5b and c, respectively. It is observed that $f_2$ = 57% and 56% at pH = 3.04 and 4.37, respectively, are closely approximate to 50% and $f_2$ = 69% at pH = 2.05 is slightly higher, suggesting that R110 has nearly equal partition in different regions in the PDMAPS–P2VP dense coacervates as an inert molecular probe for the coacervates. However, $D_{slow}$ is much smaller than $D_{fast}$ by one order of magnitude and measured to be ~28.7, 17.9, and 61.5 μm$^2$ s$^{-1}$ at pH = 2.05, 3.04, and 4.37, respectively. With measured $D_{slow}$ as well as known and fixed hydrodynamic radius, $R_H$ = 0.5 nm, of R110 as an inert molecular probe, which is independent of the polymer complex structure and medium pH, we roughly estimate the effective local viscosity, $\eta$ = ~0.015, 0.024,

 

and 0.007 Pa s of PDMAPS–P2VP dense coacervates at pH = 2.05, 3.04, and 4.37, respectively, using eqn (2). Yet it is intriguing to observe a non-monotonic change of the local viscosity of the PDMAPS–P2VP dense coacervates against pH, where the local viscosity at pH = 3.05 is higher than those at pH = 2.05 and 4.37. We attribute it to the complexity of the solution properties of weak polyelectrolytes of tunable charge fractions by pH and salt:[80,81] it is reported that the viscosity of weak polyelectrolyte solution could increase with the salt concentration at a fixed polymer concentration. Furthermore, at a fixed salt concentration, the viscosity of weak polybase solution can increase and then decrease with increasing pH due to the combined effects of decreased charge fraction yet weakened electrostatic screening caused by reduced counterion concentration. Thus we expect that the non-monotonic change of measured local viscosity of the PDMAPS–P2VP dense coacervates against pH could result from the opposite effects of P2VP concentration, charge fraction, and counterion concentration on the conformation of P2VP and the structure of the dense coacervates involving weak polyelectrolytes. To further quantify and understand the change of the local viscosity of polyelectrolyte coacervates involving weak polyelectrolytes, a future study of the scaling behavior of the P2VP chains of varied molecular weight in the coacervates of varied pH, polymer and salt concentrations could be highly desired. In this work, we solely use the local viscosity to further estimate the $R_H$ of P2VP in different dense coacervate networks without the intension to examine the viscosity of dense coacervates, assuming that the change of a local coacervate complex environment at each given polymer and salt concentration is negligible by different fluorescent probes.

Next we focus on the diffusive dynamics of f-P2VP in the PDMAPS–P2VP dense coacervates at pH = 2.05–4.37 as the measured $G(\tau)/G(0)$ is shown in Fig. 6a. Similar to the diffusion of R110 in dense coacervates, the fitting of measured $G(\tau)/G(0)$ by eqn (3) shows considerable deviation in a low $\tau$ range. Thus we have fitted the measured $G(\tau)$ with eqn (4) by setting $D_{fast,P2VP}$ equal to the diffusion of P2VP in dilute aqueous solution of the same pH.[26,51,52] The extracted $D_{slow,P2VP}$, corresponding to the diffusion of P2VP in the PDMAPS–P2VP associated network, and $f_2$ are summarized in Fig. 6b and c, respectively. The measured dynamic behaviors of f-P2VP, as well as the effective local viscosity, in the PDMAPS–P2VP dense coacervates at varied pH are also summarized in Table 2.

With the obtained local viscosity, $\eta$ of the PDMAPS–P2VP dense coacervates by $D_{slow}$ of R110 and rough assumption of the negligible effect of different fluorescent probes (R110 *versus* f-P2VP) on $\eta$, we naively derive the $R_H$ of P2VP in the PDMAPS–P2VP associated network from $D_{slow,P2VP}$ using eqn (2). Intriguingly, we observe in Fig. 7 that the $R_H$ of the P2VP chains in the associated coacervate network at pH = 2.05–3.04 appears to be approximate to that in dilute polymer solution of the same pH in agreement with the previously reported ones.[26,51,52] As illustrated in Fig. 8, the results intriguingly suggest that a swollen conformational structure of the P2VP chain is preserved upon its binding with PDMAPS at pH = 2.05–3.04 where P2VP is highly protonated. Surprisingly, $R_H$ increases considerably at pH = 4.37 beyond the FCS experimental uncertainty, suggesting a more expanded conformation of P2VP chains in the associated network. Hence, we speculate that when P2VP is highly charged at pH = 2.05–3.04, its conformation in the dense PDMAPS–P2VP associated network remains the same as an undisturbed and swollen chain upon its binding with PDMAPS. Conversely, when P2VP is less charged with increased hydrophobicity at pH = 4.37, its conformation in the dense associated network surprisingly becomes further expanded in sharp contrast to a more compact conformation for undisturbed P2VP in dilute solutions of the same pH. We attribute the further expanded conformation to enhanced "sticky" hydrophobic interactions between P2VP and PDMAPS upon coacervation instead of the hydrophobic interaction within P2VP itself, which further facilitates PDMAPS–P2VP binding by offsetting weakened electrostatic interactions. Yet, we need to point out cautiously that such conformational information is derived from a naive assumption based on unchanged local viscosity by varied fluorescent probes and the application of the Stokes–Einstein equation (eqn (2)) to dense coacervates beyond the limit of dilute polymer solution. In addition to the demand of new theoretical wisdom on coacervate microstructures, a future

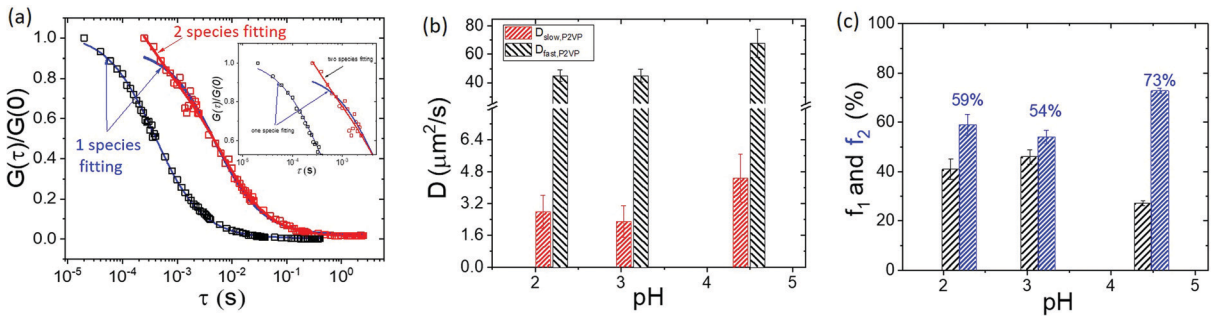


Fig. 6 (a) Normalized autocorrelation functions, $G(\tau)$, by $G(0)$ of f-P2VP in PDMAPS–P2VP dense coacervates (red squares) formed at pH = 2.05 and in dilute aqueous solution of the same $c_{KCl}$ and pH (black squares). The blue solid line indicates the fitting with eqn (2) while the red solid line indicates the fitting with eqn (4). Inset: The blowout of $G(\tau)/G(0)$ at short $\tau$ to emphasize the deviation of the fitting using eqn (3). (b) Obtained $D_{slow,P2VP}$ (red column) in the PDMAPS–P2VP associative network from the fitting of $G(\tau)/G(0)$ using eqn (4) based on the set values of $D_{fast,\ P2VP}$ (black column). (c) Fitting parameters $f_1$ (black column) and $f_2$ (blue column) corresponding to $D_{fast,P2VP}$ and $D_{slow,P2VP}$, respectively.

Table 2 List of measured $\eta$, $D_{fast,P2VP}$, $D_{slow,P2VP}$, and $f_2$ of f-P2VP in PDMAPS–P2VP dense coacervates at varied pH

| | $\eta$ (Pa s) of dense coacervate (Pa s) | $D_{fast}$ of f-P2VP in dense coacervate ($\mu m^2\ s^{-1}$) | $D_{slow}$ of f-P2VP in dense coacervate ($\mu m^2\ s^{-1}$) | $f_2$ corresponding to $D_{slow}$ (%) |
|---|---|---|---|---|
| pH = 2.05 | 0.015 | 43.0 | 2.8 | 59 |
| pH = 3.04 | 0.024 | 43.8 | 2.2 | 54 |
| pH = 4.37 | 0.007 | 67.3 | 4.4 | 73 |

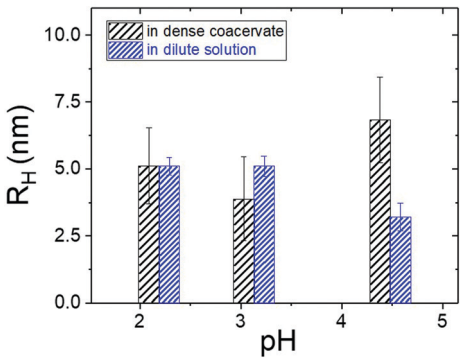


Fig. 7 $R_H$ of f-P2VP in PDMAPS–P2VP dense coacervates (black column) and in dilute solution (blue column) against solution pH.

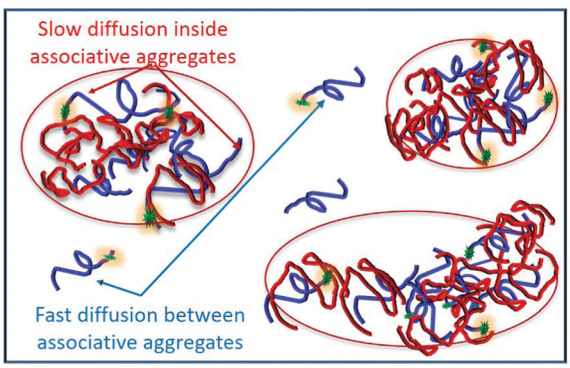


Fig. 8 Schematic illustration of f-P2VP in different regions of dense coacervates. Red circles illustrate f-P2VP diffusion in PDMAPS–P2VP associative aggregates, in contrast to f-P2VP diffusion between associative aggregates outside red circles.

study of the scaling behavior of polyelectrolyte chains in dense polyelectrolyte coacervates is warranted to further understand the structural dynamics of polyelectrolytes upon coacervation.

## Conclusions

In summary, coacervate formation between zwitterionic PDMAPS and cationic weak polyelectrolyte P2VP in KCl aqueous solutions exhibits a strong dependence on pH. The upper critical salt concentration for liquid–liquid separating PDMAPS–P2VP coacervation decreases with increasing solution pH, which is attributed to the reduced charge fraction and the increased hydrophobicity of P2VP in aqueous media. Thus, the thermodynamic landscape in terms of relative entropic to enthalpic contribution, which underlies PDMAPS–P2VP complex coacervation, is speculated to shift with pH variance. At low pH = 2.05–3.04 where P2VP is highly protonated, and the binding between PDMAPS and P2VP is similar to electrostatic induced association between the conventional polyanion and polycation, leading to entropy-driven ion pairing for PDMAPS–P2VP coacervation due to the release of counterions in a similar fashion to that reported previously for oppositely charged polyelectrolyte coacervation. The composition analysis in this pH range clearly supports the entropy-driven coacervation: higher P2VP and lower KCl concentration in dense coacervates than their respective initial ones before mixing are observed in contrast to lower P2VP and higher KCl concentration in the supernatant. Conversely, at higher pH = 4.37 where P2VP becomes considerably less protonated, the concentration difference between the dense and supernatant phases for both P2VP and KCl cases is much narrowed, suggesting that the entropic contribution to PDMAPS–P2VP coacervation is reduced. Yet, both the yielding volume fraction and water content of PDMAPS–P2VP dense coacervates are increased with increasing pH, suggesting varied PDMAPS–P2VP associative interactions and structures. Furthermore, a strong pH-dependent conformational structure of the P2VP chains in PDMAPS–P2VP dense coacervates is observed: at low pH = 2.05–3.04, the P2VP chains in the dense coacervate appear to exhibit a similar undisturbed swollen structure to that in dilute aqueous solutions of the same salt concentration and pH. Surprisingly, P2VP chains at pH = 4.37 with a resulting lower protonation degree seem to adopt a more extended conformational structure in the dense coacervate, in contrast to chain compaction as observed in dilute aqueous solution. Such a further expanded chain conformation of less charged P2VP in dense coacervates could be attributed to the enhanced hydrophobic interaction between P2VP and PDMAPS, instead of P2VP itself, for facilitating their binding upon coacervation. Put together, our results suggest that the enthalpic contribution to PDMAPS–P2VP coacervation could be increased, resulting from the enhanced hydrophobic interaction between PDMAPS and P2VP chains with increased pH. Hence, it gives further insight into the modification of the thermodynamic landscape underlying the formation and dynamic structures of polyelectrolyte coacervates when weak polyelectrolytes of tunable charge fraction are involved.

## Conflicts of interest

There are no conflicts to declare.

## Acknowledgements

The authors acknowledge the financial support from the National Science Foundation (NSF CMMI-1914436) for this work.

## References


1 C. P. Brangwynne and A. A. Hyman, The Origin of Life, *Nature*, 2012, **491**(7425), 524–525.

2 C. E. Sing and S. L. Perry, Recent progress in the science of complex coacervation, *Soft Matter*, 2020, **16**, 2885–2914.

3 F. Cousin, J. Gummel, D. Ung and F. Boue, Polyelectrolyte-protein complexes: Structure and conformation of each specie revealed by SANS, *Langmuir*, 2005, **21**, 9675–9688.

4 A. B. Kayitmazer, H. B. Bohidar, K. W. Mattison, A. Bose, J. Sarkar, A. Hashidzume, P. S. Russo, W. Jaeger and P. L. Dubin, Mesophase separaton and probe dynamics in protein-polyelectrolyte coacervates, *Soft Matter*, 2007, **3**, 1064–1076.

5 Y. Anraku, A. Kishimura, M. Kamiya, S. Tanaka, T. Nomoto, K. Toh, Y. Matsumoto, S. Fukushima, D. Sueyoshi, M. R. Kano, Y. Urano, N. Nishiyama and K. Kataoka, Systemically Injectable Enzyme-Loaded Polyion Complex Vesicles as In Vivo Nanoreactors Functioning in Tumors, *Angew. Chem., Int. Ed.*, 2016, **55**(2), 560–565.

6 C. H. Kuo, L. Leon, E. J. Chung, R. T. Huang, T. J. Sontag, C. A. Reardon, G. S. Getz, M. Tirrell and Y. Fang, Inhibition of atherosclerosis-promoting microRNAs via targeted polyelectrolyte complex micelles, *J. Mater. Chem. B*, 2014, **2**(46), 8142–8153.

7 M. von der Luhe, A. Weidner, S. Dutz and F. H. Schacher, Reversible Electrostatic Adsorption of Polyelectrolytes and Bovine Serum Albumin onto Polyzwitterion-Coated Magnetic Multicore Nanoparticles: Implications for Sensing and Drug Delivery, *ACS Appl. Nano Mater.*, 2018, **1**(1), 232–244.

8 D. S. Hwang, H. B. Zeng, A. Srivastava, D. V. Krogstad, M. Tirrell, J. N. Israelachvili and J. H. Waite, Viscosity and interfacial properties in a mussel-inspired adhesive coacervate, *Soft Matter*, 2010, **6**(14), 3232–3236.

9 R. J. Stewart, C. S. Wang and H. Shao, Complex coacervates as a foundation for synthetic underwater adhesives, *Adv. Colloid Interface Sci.*, 2011, **167**(1–2), 85–93.

10 R. J. Stewart, C. S. Wang, I. T. Song and J. P. Jones, The role of coacervation and phase transitions in the sandcastle worm adhesive system, *Adv. Colloid Interface Sci.*, 2017, **239**, 88–96.

11 N.-N. Deng, Complex coacervates as artificial membraneless organelles and protocells, *Biomicrofluidics*, 2020, **14**, 051301.

12 B. Jing, D. Xu, X. Wang and Y. Zhu, Multiresponsive, critical gel behaviors of polyzwitterion–polyoxometalate coacervate complexes, *Macromolecules*, 2018, **51**(22), 9405–9411.

13 C. J. Lee, H. Y. Wu, Y. Hu, M. Young, H. F. Wang, D. Lynch, F. J. Xu, H. B. Cong and G. Cheng, Ionic Conductivity of Polyelectrolyte Hydrogels, *ACS Appl. Mater. Interfaces*, 2018, **10**(6), 5845–5852.

14 H. Lee, E. Puodziukynaite, Y. Zhang, J. C. Stephenson, L. J. Richter, D. A. Fischer, D. M. DeLongchamp, T. Emrick and A. L. Briseno, Poly(sulfobetaine methacrylate)s as Electrode Modifiers for Inverted Organic Electronics, *J. Am. Chem. Soc.*, 2015, **137**(1), 540–549.

15 J. van der Gucht, E. Spruijt, M. Lemmers and M. A. C. Stuart, Polyelectrolyte complexes: Bulk phases and colloidal systems, *J. Colloid Interface Sci.*, 2011, **361**, 407–422.

16 J. Fu and J. B. Schlenoff, Driving Forces for Oppositely Charged Polyion Association in Aqueous Solutions: Enthalpic, Entropic, but Not Electrostatic, *J. Am. Chem. Soc.*, 2016, **138**, 980–990.

17 Z. Y. Ou and M. Muthukumar, Entropy and enthalpy of polyelectrolyte complexation: Langevin dynamics simulations, *J. Chem. Phys.*, 2006, **124**(15), 154902.

18 V. S. Rathee, A. J. Zervoudakis, H. Sidky, B. J. Sikora and J. K. Whitmer, Weak polyelectrolyte complexation driven by associative charging, *J. Chem. Phys.*, 2018, **148**(11), 114901.

19 J. B. Schlenoff, M. Yang, Z. A. Digby and Q. F. Wang, Ion Content of Polyelectrolyte Complex Coacervates and the Donnan Equilibrium, *Macromolecules*, 2019, **52**(23), 9149–9159.

20 M. Yang, Z. A. Digby and J. B. Schlenoff, Precision Doping of Polyelectrolyte Complexes: Insight on the Role of Ions, *Macromolecules*, 2020, **53**(13), 5465–5474.

21 M. Yang, J. B. Shi and J. B. Schlenoff, Control of Dynamics in Polyelectrolyte Complexes by Temperature and Salt, *Macromolecules*, 2019, **52**(5), 1930–1941.

22 P. K. Jha, P. S. Desai, J. Y. Li and R. G. Larson, pH and Salt Effects on the Associative Phase Separation of Oppositely Charged Polyelectrolytes, *Polymers*, 2014, **6**(5), 1414–1436.

23 V. S. Rathee, H. Sidky, B. J. Sikora and J. K. Whitmer, Role of Associative Charging in the Entropy-Energy Balance of Polyelectrolyte Complexes, *J. Am. Chem. Soc.*, 2018, **140**(45), 15319–15328.

24 A. M. Rumyantsev, E. B. Zhulina and O. V. Borisov, Complex coacervate of weakly charged polyelectrolytes: Diagram of states, *Macromolecules*, 2018, **51**, 3788–3801.

25 E. Raphael and J. F. Joanny, Annealed and quenched polyelectrolytes, *Europhys. Lett.*, 1990, **13**(7), 623–628.

26 S. Q. Wang, S. Granick and J. Zhao, Charge on a weak polyelectrolyte, *J. Chem. Phys.*, 2008, **129**, 24.

27 J. Huang, F. J. Morin and J. E. Laaser, Charge-density-dominated phase behavior and viscoelasticity of polyelectrolyte complex coacervates, *Macromolecules*, 2019, **52**, 4957–4967.

28 J. Lou, S. Friedowitz, J. Qin and Y. Xia, Tunable coacervation of well-defined homologous polyanions and polycations by local polarity, *ACS Cent. Sci.*, 2019, **5**, 549.

29 I. T. Song and R. J. Stewart, Complex coacervation of Mg(ii) phospho-polymethacrylate, a synthetic analog of sandcastle worm adhesive phosphoproteins, *Soft Matter*, 2018, **14**, 379–386.

30 M. Ferreira, B. Jing, A. Lorenzana and Y. Zhu, Effect of polyampholyte net charge on complex coacervation between polyampholytes and inorganic polyoxometalate giant anions, *Soft Matter*, 2020, **45**, 10280–10289.

31 B. Jing, J. Qiu and Y. Zhu, Organic–inorganic macroion coacervate complexation, *Soft Matter*, 2017, **13**(28), 4881–4889.

32 K. Sadman, Q. Wang, Y. Chen, B. Keshavarz, Z. Jiang and K. R. Shull, Influence of hydrophobicity on polyelectrolyte complexation, *Macromolecules*, 2017, **50**, 9417–9426.

33 L. Li, S. Srivastava, M. Andreev, A. B. Marciel, J. J. de Pablo and M. V. Tirrell, Phase Behavior and Salt Partitioning in

Polyelectrolyte Complex Coacervates, *Macromolecules*, 2018, **51**, 2988–2995.

34 A. B. Marciel, S. Srivastava and M. V. Tirrell, Structure and rheology of polyelectrolyte complex coacervates, *Soft Matter*, 2018, **14**(13), 2454–2464.

35 D. Priftis, K. Megley, N. Laugel and M. Tirrell, Complex coacervation of poly(ethylene-imine)/polypeptide aqueous solutions: Thermodynamic and rheological characterization, *J. Colloid Interface Sci.*, 2013, **398**, 39–50.

36 E. Kizilay, D. Seeman, Y. Yan, X. Du, P. L. Dubin, L. Donato-Capel, L. Bovetto and C. Schmitt, Structure of Bovine [small beta]-Lactoglobulin-lactoferrin Coacervates, *Soft Matter*, 2014, **10**(37), 7262–7268.

37 D. V. Krogstad, S.-H. Choi, N. A. Lynd, D. J. Audus, S. L. Perry, J. D. Gopez, C. J. Hawker, E. J. Kramer and M. V. Tirrell, Small Angle Neutron Scattering Study of Complex Coacervate Micelles and Hydrogels Formed from Ionic Diblock and Triblock Copolymers, *J. Phys. Chem. B*, 2014, **118**(45), 13011–13018.

38 S. S. Singh, V. K. Aswal and H. B. Bohidar, Structural Studies of Agar–gelatin Complex Coacervates by Small Angle Neutron Scattering, Rheology and Differential Scanning Calorimetry, *Int. J. Biol. Macromol.*, 2007, **41**(3), 301–307.

39 X. Y. Wang, Y. Q. Li, Y. W. Wang, J. Lal and Q. R. Huang, Microstructure of beta-lactoglobulin/pectin coacervates studied by small-angle neutron scattering, *J. Phys. Chem. B*, 2007, **111**(3), 515–520.

40 J. H. E. Hone, A. M. Howe and T. Cosgrove, A small-angle neutron scattering study of the structure of gelatin/polyelectrolyte complexes, *Macromolecules*, 2000, **33**(4), 1206–1212.

41 E. Spruijt, F. A. M. Leermakers, R. Fokkink, R. Schweins, A. A. van Well, M. A. C. Stuart and J. van der Gucht, Structure and Dynamics of Polyelectrolyte Complex Coacervates Studied by Scattering of Neutrons, X-rays, and Light, *Macromolecules*, 2013, **46**(11), 4596–4605.

42 K.-Y. Huang, H. Y. Yoo, Y. Jho, S. Han and D. S. Hwang, Bicontinuous Fluid Structure with Low Cohesive Energy: Molecular Basis for Exceptionally Low Interfacial Tension of Complex Coacervate Fluids, *ACS Nano*, 2016, **10**(5), 5051–5062.

43 S. Kim, J. Huang, Y. Lee, S. Dutta, H. Y. Yoo, Y. M. Jung, Y. S. Jho, H. B. Zeng and D. S. Hwang, Complexation and coacervation of like-charged polyelectrolytes inspired by mussels, *Proc. Natl. Acad. Sci. U. S. A.*, 2016, **113**(7), E847–E853.

44 E. Kizilay, A. D. Dinsmore, D. A. Hoagland, L. Sun and P. L. Dubin, Evolution of hierarchical structures in polyelectrolyte–micelle coacervates, *Soft Matter*, 2013, **9**(30), 7320–7332.

45 H. Le Ferrand, M. Duchamp, B. Gabryelczyk, H. Cai and A. Miserez, Time-Resolved Observations of Liquid–Liquid Phase Separation at the Nanoscale Using in Situ Liquid Transmission Electron Microscopy, *J. Am. Chem. Soc.*, 2019, **141**(17), 7202–7210.

46 Y. Jho, H. Y. Yoo, Y. Lin, S. Han and D. S. Hwang, Molecular and structural basis of low interfacial energy of complex coacervates in water, *Adv. Colloid Interface Sci.*, 2017, **239**, 61–73.

47 F. Weinbreck, H. S. Rollema, R. H. Tromp and C. G. de Kruif, Diffusivity of whey protein and gum arabic in their coacervates, *Langmuir*, 2004, **20**(15), 6389–6395.

48 M. Tekaata, D. Bütergerdsa, M. Schönhoffa, A. Feryb and C. Cramer, Scaling properties of the shear modulus of polyelectrolyte complex coacervates: A time-pH superposition principle, *Phys. Chem. Chem. Phys.*, 2015, **17**, 22552–22556.

49 A. B. Lowe and C. L. McCormick, Synthesis and Solution Properties of Zwitterionic Polymers, *Chem. Rev.*, 2002, **102**(11), 4177–4190.

50 P. Mary, D. D. Bendejacq, M. P. Labeau and P. Dupuis, Reconciling low- and high-salt solution behavior of sulfobetaine polyzwitterions, *J. Phys. Chem. B*, 2007, **111**(27), 7767–7777.

51 S. Q. Wang and J. Zhao, First-order conformation transition of single poly(2-vinylpyridine) molecules in aqueous solutions, *J. Chem. Phys.*, 2007, **126**, 9.

52 S. Q. Wang and Y. Zhu, Conformation transition and electric potential of single weak polyelectrolyte: molecular weight dependence, *Soft Matter*, 2011, **7**(16), 7410–7415.

53 B. Jing, M. Ferreira, K. Lin, R. Li, B. M. Yavitt, J. Qiu, M. Fukuto and Y. Zhu, Ultrastructure of Critical-Gel-like Polyzwitterion−Polyoxometalate Complex Coacervates: Effects of Temperature, Salt Concentration, and Shear, *Macromolecules*, 2020, **53**, 10972–10980.

54 B. Valley, B. Jing, M. Ferreira and Y. Zhu, Rapid and efficient coacervate extraction of cationic industrial dyes from wastewater, *ACS Appl. Mater. Interfaces*, 2019, **11**, 7472–7478.

55 I. Chalari, S. Pispas and N. Hadjichristidis, Controlled free-radical polymerization of 2-vinylpyridine in the presence of nitroxides, *J. Polym. Sci., Part A: Polym. Chem.*, 2001, **39**(17), 2889–2895.

56 I. F. Pierola, N. J. Turro and P. L. Kuo, Proton-transfer reactions of poly(2-vinylpyridine) in the 1st single excited-state, *Macromolecules*, 1985, **18**(3), 508–511.

57 C. Qu, Y. Shi, B. X. Jing, H. F. Gao and Y. X. Zhu, Probing the Inhomogeneous Charge Distribution on Annealed Polyelectrolyte Star Polymers in Dilute Aqueous Solutions, *ACS Macro Lett.*, 2016, **5**(3), 402–406.

58 H. M. C. Vink, A New Convenient Method for the Synthesis of Poly(styrenesulfonic acid), *Makromol. Chem.*, 1981, **182**, 279–281.

59 F. Wang, J. F. Yang and J. Zhao, Understanding anti-polyelectrolyte behavior of a well-defined polyzwitterion at the single-chain level, *Polym. Int.*, 2015, **64**(8), 999–1005.

60 T. Wang, R. Kou, H. Liu, L. Liu, G. Zhang and G. Liu, Anion Specificity of Polyzwitterionic Brushes with Different Carbon Spacer Lengths and Its Application for Controlling Protein Adsorption, *Langmuir*, 2016, **32**(11), 2698–2707.

61 Water analysis, in *Practical Environmental Analysis*, ed. M. Radojević and V. N. Bashkin, Royal Society of Chemistry, 1999, pp. 138–273.

62 L. Yoder, Adaptation of the Mohr Volumetric Method to General Determinations of Chlorine, *J. Ind. Eng. Chem.*, 1919, **11**(8), 755.

 

63 K. G. Kehl and V. R. Meyer, Argentometric Titration for the Determination of Liquid Chromatographic Injection Reproducibility, *Anal. Chem.*, 2001, **73**(1), 131–133.
64 D. Magde, W. W. Webb and E. Elson, Thermodynamic fluctuations in a reacting system - measurement by fluorescence correlation spectroscopy, *Phys. Rev. Lett.*, 1972, **29**(11), 705–708.
65 R. Rigler, U. Mets, J. Widengren and P. Kask, Fluorewcence correlation spectroscopy with high count rate and low-background -analysis of translational diffusion, *Eur. Biophys. J.*, 1993, **22**(3), 169–175.
66 E. Spruijt, A. H. Westphal, J. W. Borst, M. A. C. Stuart and J. van der Gucht, Binodal compositions of polyelectrolyte complexes, *Macromolecules*, 2010, **43**, 6476–6484.
67 P. M. Biesheuvel and M. A. C. Stuart, Cylindrical cell model for the electrostatic free energy of polyelectrolyte complexes, *Langmuir*, 2004, **20**(11), 4764–4770.
68 R. Chollakup, W. Smitthipong, C. D. Eisenbach and M. Tirrell, Phase behavior and coacervation of aqueous poly(acrylic acid)-poly(allylamine) solutions, *Macromolecules*, 2010, **43**(5), 2518–2528.
69 B. M. Johnston, C. W. Johnston, R. A. Letteri, T. K. Lytle, C. E. Sing, T. Emrick and S. L. Perry, The effect of comb architecture on complex coacervation, *Org. Biomol. Chem.*, 2017, **15**(36), 7630–7642.
70 F. Weinbreck and R. H. W. Wientjes, Rheological properties of whey protein/gum arabic coacervates, *J. Rheol.*, 2004, **48**(6), 1215–1228.
71 B. Jing, M. Ferreira, Y. Gao, C. Wood, R. P. Li, M. Fukuto, T. Liu and Y. Zhu, Unconventional Complex Coacervation between Neutral Polymer and Inorganic Polyoxometalate in Aqueous Solution via Direct Water Mediation, *Macromolecules*, 2019, **52**(21), 8275–8284.
72 C. Tsitsilianis, I. Iliopoulos and G. Ducouret, An associative polyelectrolyte end-capped with short polystyrene chains. Synthesis and rheological behavior, *Macromolecules*, 2000, **33**, 2936–2943.
73 Z. Zhang, Q. Chen and R. Colby, Dynamics of associative polymers, *Soft Matter*, 2018, **14**, 2961–2977.
74 *Physics of Polymer Gels*, ed. T. Sakai, Wiely-VCH Verlag GmbH &Co, 2020.
75 J. B. Schlenoff, M. Yang, Z. A. Digby and Q. F. Wang, Ion Content of Polyelectrolyte Complex Coacervates and the Donnan Equilibrium, *Macromolecules*, 2019, **52**, 9149–9159.
76 S. Q. Wang, B. Jing and Y. Zhu, Single molecule diffusion on hard, soft and fluid surfaces, *RSC Adv.*, 2012, **2**(9), 3835–3843.
77 V. E. Goodrich, E. Connor, S. Q. Wang, J. F. Yang, J. Zhao and Y. Zhu, AC-electrokinetic manipulation and controlled encapsulate release of surfactant based micelles, *Soft Matter*, 2013, **9**, 5052–5060.
78 A. Shakya and J. T. King, Non-Fickian molecular transport in protein-DNA droplets, *ACS Macro Lett.*, 2018, **7**, 1220–1225.
79 C. L. Cooper, P. L. Dubin, A. B. Kayitmazer and S. Turksen, Polyelectrolyte–protein complexes, *Curr. Opin. Colloid Interface Sci.*, 2005, **10**, 52–78.
80 N. B. Wyatt, C. M. Gunther and M. W. Liberatore, Increasing viscosity in entangled polyelectrolyte solutions by the addition of salt, *Polymer*, 2011, **52**, 2437–2444.
81 G. Weill, Viscosity and scattering of very weakly charged polyelectrolytes, *Biophys. Chem.*, 1991, **41**, 1–8.